Spectral models for solar-scaled and α-enhanced stellar populations

P. Coelho,[1,3,4]★ G. Bruzual,[2]★ S. Charlot,[1]★ A. Weiss,[3]★ B. Barbuy[4]★
and J. W. Ferguson[5]★

[1]*Institut d'Astrophysique, CNRS, Université Pierre et Marie Curie, 98 bis Bd Arago, 75014 Paris, France*
[2]*Centro de Investigaciones de Astronomia (CIDA), Merida, Venezuela*
[3]*Max-Planck-Institute für Astrophysik, Karl-Schwarzschild-Strasse 1, 85740 Garching bei München, Germany*
[4]*Universidade de São Paulo, IAG, Rua do Matão 1226, São Paulo 05508-900, Brazil*
[5]*Department of Physics, Wichita State University, Wichita, KS 67260-0032, USA*

ABSTRACT

We present the first models allowing one to explore in a consistent way the influence of changes in the α-element-to-iron abundance ratio on the high-resolution spectral properties of evolving stellar populations. The models cover the wavelength range from 3000 Å to 1.34 μm at a constant resolution of full width at half-maximum (FWHM) = 1 Å and a sampling of 0.2 Å, for overall metallicities in the range $0.005 \leqslant Z \leqslant 0.048$ and for stellar population ages between 3 and 14 Gyr. These models are based on a recent library of synthetic stellar spectra and a new library of stellar evolutionary tracks, both computed for three different iron abundances ([Fe/H] = −0.5, 0.0 and 0.2) and two different α-element-to-iron abundance ratios ([α/Fe] = 0.0 and 0.4). We expect our fully synthetic models to be primarily useful for evaluating the differential effect of changes in the α/Fe ratio on spectral properties such as broad-band colours and narrow spectral features. In addition, we assess the accuracy of absolute model predictions in two ways: first, by comparing the predictions of models for scaled-solar metal abundances ([α/Fe] = 0.0) to those of existing models based on libraries of observed stellar spectra; and secondly, by comparing the predictions of models for α-enhanced metal abundances ([α/Fe] = 0.4) to observed spectra of massive early-type galaxies in the Sloan Digital Sky Survey Data Release 4. We find that our models predict accurate strengths for those spectral indices that are strongly sensitive to the abundances of Fe and α elements. The predictions are less reliable for the strengths of other spectral features, such as those dominated by the abundances of C and N, as expected from the fact that the models do not yet allow one to explore the influence of these elements in an independent way. We conclude that our models are a powerful tool for extracting new information about the chemical properties of galaxies for which high-quality spectra have been gathered by modern surveys.

Key words: stars: atmospheres – stars: evolution – galaxies: abundances – galaxies: evolution – galaxies: stellar content.

1 INTRODUCTION

The chemical abundance patterns in the spectra of stellar populations are direct tracers of the histories of star formation and chemical enrichment of galaxies. These patterns are sensitive to the different relative amounts of metals produced on short time-scale ($\sim 10^7$ yr) by Type II supernovae and on longer time-scales (a few $\times 10^9$ yr) by Type Ia supernovae. In recent years, modern spectroscopic galaxy surveys have gathered hundreds of thousands of high-quality spectra, in which such signatures can be analysed (e.g. Colless et al. 2001; Adelman-McCarthy et al. 2006). We must be able to interpret these spectral signatures to constrain the past histories of star formation and chemical enrichment of the galaxies.

Evolutionary stellar population synthesis, i.e. the modelling of the spectral energy distribution (SED) emitted by evolving stellar populations, is a natural approach to studying the stellar content of galaxies. A current limitation in this area is that all models of high-resolution galaxy spectra rely on the spectral properties of stars in our own Galaxy. This implies that the models are tuned to the specific chemistry and star formation history of the Milky Way. This is restraining, because stars in external galaxies are known to exhibit

★E-mail: pcoelho@iap.fr (PC); bruzual@cida.ve (GB); charlot@iap.fr (SC); weiss@mpa-garching.mpg.de (AW); barbuy@astro.iag.usp.br (BB); jason.ferguson@wichita.edu (JWF)

other abundance patterns. For example, in massive early-type galaxies, light α elements (O, Ne, Mg, Si, S, Ca and Ti, produced mainly by Type II supernovae) are typically more abundant relative to iron (produced mainly by Type Ia supernovae) than in the Milky Way disc (e.g. Worthey, Faber & Gonzalez 1992). Hence, widely used population synthesis models such as those developed by Vazdekis (1999), Bruzual & Charlot (2003) and Le Borgne et al. (2004), should be applied with caution to the analysis of high-resolution spectra of external galaxies.

Pioneer population synthesis models have been developed to quantify the influence of changes in metal abundance ratios on the strengths of 'Lick/IDS indices' that measure a number of strong absorption features in galaxy spectra (see Burstein et al. 1984; Trager et al. 1998; Worthey et al. 1994). These models rely on a semi-empirical approach, which consists in applying theoretical response functions to empirical fitting functions in order to predict the strengths of Lick/IDS indices with variable abundance ratios (e.g., Trager et al. 2000; Thomas, Maraston & Bender 2003b; Proctor, Forbes & Beasley 2004; Tantalo & Chiosi 2004; Lee & Worthey 2005; Annibali et al. 2007; Schiavon 2007). The empirical *fitting functions* describe how spectral indices vary as a function of the stellar parameters effective temperature $T_{\rm eff}$, gravity $\log g$, metallicity [Fe/H] and, sometimes, abundance [X/Fe] of another element relative to iron (e.g. Diaz, Terlevich & Terlevich 1989; Jorgensen, Carlsson & Johnson 1992; Borges et al. 1995; Worthey et al. 1994; Schiavon 2007). Theoretical *response functions* (e.g. Tripicco & Bell 1995; Houdashelt et al. 2002; Korn, Maraston & Thomas 2005) quantify how the indices change due to variations of individual chemical elements. Typically, these response functions are calculated only for three combinations of $T_{\rm eff}$ and $\log g$, which correspond to a main-sequence (MS) star, a turn-off star and a red giant star for a 5-Gyr-old stellar population. All other stars of a same evolutionary phase are assumed to respond in the same way to abundance variations. Alternatively, theoretical fitting functions with explicit dependence on α/Fe (Barbuy et al. 2003) can be employed to compute α-enhanced models (Mendes de Oliveira et al. 2005). By construction, all these models are limited to the study of a few selected spectral indices.

Recent progress in the modelling of high-resolution stellar spectra is opening the door to a new kind of models, in which the effects of abundance variations can be studied at any wavelength. This is enabled by the publication of several libraries of theoretical, high-resolution stellar spectra for both scaled-solar and α-enhanced chemical mixtures (Coelho et al. 2005; Gustafsson et al. 2003; Malagnini et al. 2005; Munari et al. 2005; Brott & Hauschildt 2005). Libraries with scaled-solar mixtures have already been used to construct high-resolution population synthesis relying purely on theoretical spectra (e.g. Delgado et al. 2005; Zhang, Li & Han 2005). Such spectra are easier to handle than observed spectra because they have arbitrary wavelength resolution, infinite signal-to-noise ratio (S/N), and they correspond to well-defined stellar parameters. The disadvantage of synthetic spectra is that they are limited by the uncertainties inherent in the underlying model atmosphere calculations (such as the neglect of departures from local thermodynamical equilibrium and of chromospheric, three-dimensional and sphericity effects) and by potential inaccuracies in the parameters of the atomic and molecular transitions line lists (line wavelengths, energy levels, oscillator strengths and damping parameters; see e.g. Kurucz 2006). Despite these limitations, theoretical model spectra represent a unique opportunity to study the response of any spectral feature to abundance variations in galaxy spectra. For such a study to be meaningful, one must also include the effects of abundance variations on

Table 1. Chemical composition of the models.

Label	X	Y	Z	[Fe/H]	[α/Fe]	[$Z/Z_\odot$]
$m05p00$	0.743	0.251	0.005	−0.5	0.0	−0.5
$m05p04$	0.739	0.250	0.011	−0.5	0.4	−0.2
$p00p00$	0.718	0.266	0.017	0.0	0.0	0.0
$p00p04$	0.679	0.289	0.032	0.0	0.4	0.3
$p02p00$	0.708	0.266	0.026	0.2	0.0	0.2
$p02p04$	0.642	0.310	0.048	0.2	0.4	0.5

the evolution of the stars, which cannot be neglected for metallicities larger than about half solar (Weiss, Peletier & Matteucci 1995; Salaris & Weiss 1998; Salasnich et al. 2000; VandenBerg et al. 2000).

In this paper, we combine the library of synthetic stellar spectra recently published by Coelho et al. (2005, hereafter C05) with a new library of stellar evolutionary tracks computed by Weiss et al. (2007), to predict the high-resolution spectral properties of evolving stellar populations with different metallicities and α/Fe abundance ratios. For the purpose of this study, we extend the range of stellar effective temperatures and improve the spectrophotometric calibration of the C05 library (see Sections 3.1–3.2). A salient feature of our model is that both the library of synthetic stellar spectra and that of stellar evolutionary tracks are computed for the same mixtures of chemical elements, listed in Table 1. At fixed [Fe/H], we assume that in the 'α-enhanced' model, the abundances of all classical α elements, i.e. O, Ne, Mg, Si, S, Ca and Ti, are increased by 0.4 dex relative to the scaled-solar model.[1] We adopt the Bruzual & Charlot (2003, hereafter BC03) code to compute the spectral evolution of stellar populations based on these libraries of stellar spectra and evolutionary tracks. The resulting models cover the wavelength range from 3000 Å to 1.34 μm at a constant resolution of FWHM = 1 Å and a sampling of 0.2 Å, for overall metallicities in the range $0.005 \leqslant Z \leqslant 0.048$ and for stellar population ages between 3 and 14 Gyr.

The paper is organized as follows. In Sections 2 and 3 below, we describe in detail the main two ingredients of our models: the library of stellar evolutionary tracks and the library of synthetic stellar spectra, respectively. Section 4 provides an overview of the stellar population synthesis code. In Section 5, we make a first assessment of the performance of our fully synthetic models by comparing the predictions for scaled-solar stellar populations to those of models based on libraries of observed stellar spectra. Then, in Section 6, we explore the effects of the α enhancement on the spectroscopic and photometric properties of stellar populations. We show that the spectra of α-enhanced models compare well to observed spectra of massive early-type galaxies in the Sloan Digital Sky Survey Data Release 4 (SDSS-DR4). We also compare our predictions for Lick-index strengths for different α/Fe with respect to those of previous models. Section 7 summarizes our results.

---

[1] There is no consensus in the literature on whether it is more appropriate to fix the iron abundance [Fe/H] or the total metal abundance [Z/H] when exploring models with different α/Fe (see e.g. the different methods in Proctor & Sansom 2002). C05, following Castelli & Kurucz (2003), fix [Fe/H] when computing theoretical stellar spectra for different α/Fe. We adopt the same convention, which is motivated by the fact that in high-resolution stellar spectroscopic studies, [Fe/H] can be directly derived from the equivalent widths of Fe lines. The total metallicity [Z/H] is a less accurate value, being computed based on assumptions for those elements whose abundances could not be derived.

2 STELLAR EVOLUTION MODELS

Above approximately half solar metallicity, the α enhancement changes the evolutionary time-scales and isochrones in non-negligible ways (Weiss et al. 1995; Salaris & Weiss 1998; Salasnich et al. 2000; VandenBerg et al. 2000). At fixed total metallicity, α-enhanced isochrones tend to be warmer and slightly fainter than solar-scaled ones, while at fixed [Fe/H] the increased total metallicity of the α-enhanced models leads to cooler colours and fainter brightness. It is crucial therefore that single stellar population (SSP) models include tracks computed with proper abundance patterns. And it is important that the assumptions for the abundance pattern are consistent among the ingredients.

2.1 Stellar evolution code

The stellar evolution models for this project were calculated using the Garching Stellar Evolution Code, which was described in detail in Weiss & Schlattl (2000). We use the OPAL equation of state (Rogers, Swenson & Iglesias 1996), nuclear reaction rates mainly from Caughlan et al. (1985), Caughlan & Fowler (1988) and Adelberger et al. (1998), neutrino emission rates from Itoh et al. (1996) and Haft, Raffelt & Weiss (1994). We use standard mixing-length theory with a value of $\alpha_{MLT} = 1.6$, which is obtained from a solar model calibration. We ignore any effects of overshooting and semiconvection, and diffusion is included neither in the present models nor in the solar one. The models are evolved at constant mass. They are therefore the most canonical ones possible. Inclusion of any of the effects mentioned above would introduce additional parameters and assumptions. Since the main purpose of this paper is to investigate the influence of α-element abundances, we thought it more reasonable to keep the number of assumptions as low as possible.

Element variations enter stellar models at various places, and we have taken great care to consider these as consistently as possible. The most obvious instance is the chemical mixture for the initial model. We start from the solar composition of Grevesse & Sauval (1998), adding a constant enhancement of 0.4 dex to O, Ne, Mg, Si, S, Ca and Ti. The final abundances are given in Weiss et al. (2007, table 1). The molecular weight is calculated from these abundances. Although one would like to take the detailed abundances into account also in the equation of state, this is no longer trivial. In this respect, our models are not self-consistent, as we consider only the total metallicity (and the hydrogen and helium abundances) in the calculation of the equation of state. It is generally supposed that this is a sufficiently accurate approximation.

In the nuclear network, element abundances enter explicitly the reaction rates and therefore can be taken into account straightforwardly.

Finally, and most importantly for the stellar effective temperature and therefore observed colours, spectra and line indices, the opacities have to be calculated as accurate as possible. Throughout this paper we are using Rosseland opacity tables from the OPAL web site[2] (Iglesias & Rogers 1996) for high temperatures together with low-temperature molecular opacity tables calculated by one of us (JF), employing the code by Ferguson et al. (2005). The most important feature of the final opacity tables is that they were produced for exactly the same element composition, both in the solar and α-enhanced case. Details on the implementation of opacity tables in our code can be found in Weiss et al. (2007).
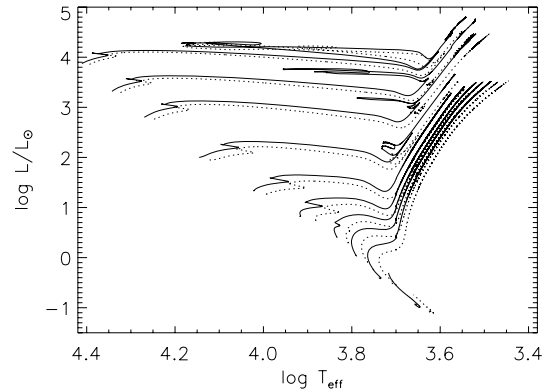

Figure 1. Evolution of models at [Fe/H] $= -0.5$ with mixture [α/Fe] $= 0.0$ (*m05p00* in Table 1; solid lines) and [α/Fe] $= 0.4$ (*m04p04*; dotted lines). For clarity, only tracks for $M/M_\odot = 0.6, 0.8, 1.0, 1.2, 1.5, 2.0, 3.0, 5.0, 7.0$ and 10.0 are shown.

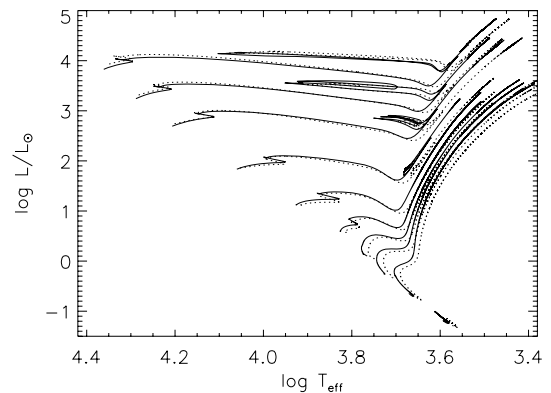**Figure 2.** As Fig. 1, but at [Fe/H] $= 0.2$ for mixtures [α/Fe] $= 0.0$ (*p02p00*; solid lines) and [α/Fe] $= 0.4$ (*p02p04*; dotted lines).

We initially intended to use the set of α-enhanced tables already available to us, which include molecular opacities by Alexander & Ferguson (1994). These data were used, for example, by Salasnich et al. (2000), and are for a slightly different element composition of varying α-enhancement factors. We assumed initially that the internal table composition differences would not affect the models significantly. However, as discussed in Weiss et al. (2007), this assumption proved to be wrong, such that we produced completely consistent and up-to-date new tables. For the effect of α-element variations on the models and isochrones, see below.

2.2 Models

We followed the evolution of low-mass stars ($M \leqslant 2\,M_\odot$) from the MS up to the core helium flash, that of intermediate mass stars ($3 \leqslant M/M_\odot \leqslant 7$) into the early asymptotic giant branch (AGB), and that of $M = 10\,M_\odot$ to the beginning of core carbon burning.

The mass grid in detail was: $M = 0.60, \ldots (0.05) \ldots, 1.20,$ 1.50, 2.00, 3.00, 5.00, 7.00, 10.00 $M_\odot$. The various compositions are given in Table 1.

In Figs 1 and 2 we show in the Hertzsprung–Russell diagram (HRD) the evolutionary tracks for mixtures of identical [Fe/H] with solar and α-enhanced metal ratios.[3] In the first case ([Fe/H] $= -0.5$)

---

[2] http://www-phys.llnl.gov/Research/OPAL.

[3] The case [Fe/H] $= 0.0$ has already been presented in Weiss et al. (2007).

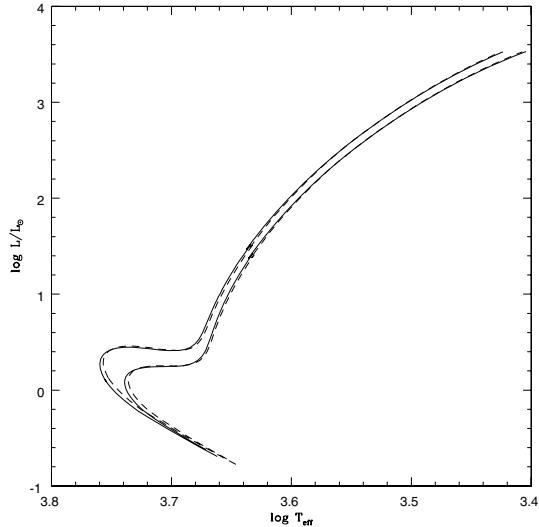**Figure 3.** Isochrones of 8 and 14 Gyr for models with $Z = 0.032$ and α enrichment, either variable (dashed lines) or constant (solid lines).

the hydrogen and helium abundances are very similar, such that the effect of the enhanced total metallicity for the α-enhanced mixture shows clearly up in lower effective temperatures and MS luminosities, and thus longer lifetimes. For example, the $1\,M_\odot$ has a turn-off age of 5.8 Gyr (solar) and 7.4 Gyr (α enhanced).

On the other hand, the comparison at [Fe/H] = 0.2 shows comparatively small differences in the HRD; also the lifetimes of the $1\,M_\odot$ star (and of the others) is quite similar (10.1 and 10.7 Gyr). The reason for this is that although the metallicity in the α-enhanced case is 0.048, compared to 0.026 of the solar-scaled case, the hydrogen content is much higher in the latter (0.708 compared to 0.642), such that the lack of opacity due to the metals is compensated for by the increased hydrogen opacity. This emphasizes the fact already mentioned in Weiss et al. (1995) that at high metallicities the detailed assumptions about the galactochemical history of the helium content becomes crucial.

Thus, the choice of helium enrichment is becoming an issue for such metal-rich systems. We decided to assume a moderate value for the helium enrichment factor $\triangle Y/\triangle Z$, starting from a primordial helium content of approximately 0.240. With this, $\triangle Y/\triangle Z$ for the solar-like mixture $(X, Z) = (0.718, 0.016)$ is 1.62 (p00p00 in Table 1), and for the corresponding α-enhanced one 1.53 (p00p04). For the other mixtures it lies between 1 and 2, with the lowest value being 0.9 for the α-rich subsolar mixture. Given the uncertainty in the solar model abundances and that of the galactic value for $\triangle Y/\triangle Z$, and the question whether this value is the same for solar-scaled and α-enriched material at identical [Fe/H], this choice is as good as any other.

Another point of uncertainty is that of the actual α-enrichment factors. As discussed in Weiss et al. (2007) the difference between a constant or variable enhancement might lead to crucial lifetime changes for stars of given mass. This is due to systematic differences in the opacities at core temperatures. However, it was also stressed that this refers to the evolution at fixed mass, but not necessarily to isochrones at fixed age. We therefore show in Fig. 3 isochrones of 8 and 14 Gyr for models with either a variable or constant α-element enhancement. The differences are not very large; e.g. the turn-off (TO) at 14 Gyr is hotter by less than 40 K, and fainter by less than 5 per cent for the variable enhancement factors. However, the TO
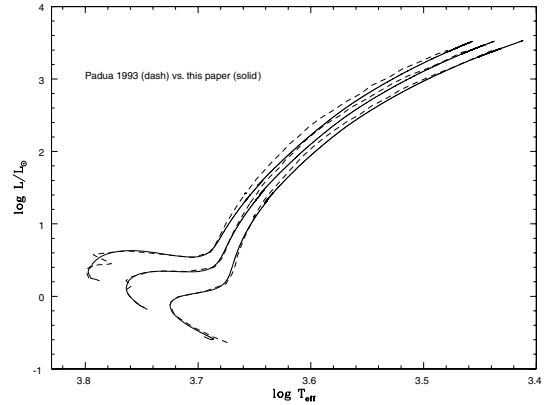

Figure 4. Comparison between Bressan et al. (1993, dashed lines) and our models (solid) for a standard mixture of $X = 0.70$, $Y = 0.28$ and $Z = 0.02$ for three stellar masses (0.8, 1.0 and $1.2\,M_\odot$).

mass is $0.05\,M_\odot$ lower. We conclude that for population synthesis aspects the influence of the rather high sensitivity of the opacities with respect to composition details is very modest and no source of concern.

Finally, for comparison, we show in Fig. 4 the tracks for a standard solar mixture of $(X, Z) = (0.70, 0.02)$ for both the Padova library (Bressan et al. 1993) and our own calculations. We compare only low-mass stars, as the higher masses are affected even more by the different treatment of overshooting. Even then, the effect is visible in the structure around the turn-off, as our models all have only transient convective cores during the earliest few million years, while the Padova models for $M = 1.0$ and $1.2\,M_\odot$ have persistent convective cores. Otherwise, the tracks agree very well, given the fact that almost 15 yr lie between the two calculations. Only the red giant branch (RGB) temperatures differ appreciably, which can be explained by the fact that Bressan et al. (1993) did not have access to the molecular opacities by Alexander & Ferguson (1994). Also the core hydrogen burning time of these models agree within 1.5 per cent.

3 STELLAR SPECTRAL ENERGY DISTRIBUTIONS

The base of our stellar ingredient is the synthetic library by C05,[4] which is focused on the accurate reproduction of late-type stars. This library is based on the models atmospheres by Castelli & Kurucz (2003, hereafter ATLAS9), and on a refined atomic and molecular line list calibrated through several stellar spectroscopic studies (see e.g. Barbuy et al. 2003).[5] We refer the reader to C05 for details on the high-resolution spectrum calculations.

Some changes were made to the C05 library in order to better suit stellar population studies: the spectra were smoothed with a Gaussian filter and resampled, so that we obtain spectra with a constant resolution of FWHM = 1 Å and a sampling of $0.2\,\text{Å pix}^{-1}$; additional

---

[4] http://www.mpa-garching.mpg.de/PUBLICATIONS/DATA/SYNTHST-ELLIB/synthetic_stellar_spectra.html.

[5] Note on nomenclature: by *model atmosphere* we mean the run of temperature and pressures as a function of optical depth which describes the photosphere of a star. It distinguishes from *flux distribution* and *synthetic spectrum* which are the emergent fluxes calculated given a model atmosphere, whereas in general *flux distribution* corresponds to low-resolution spectrum, and *synthetic spectrum* to high resolution.
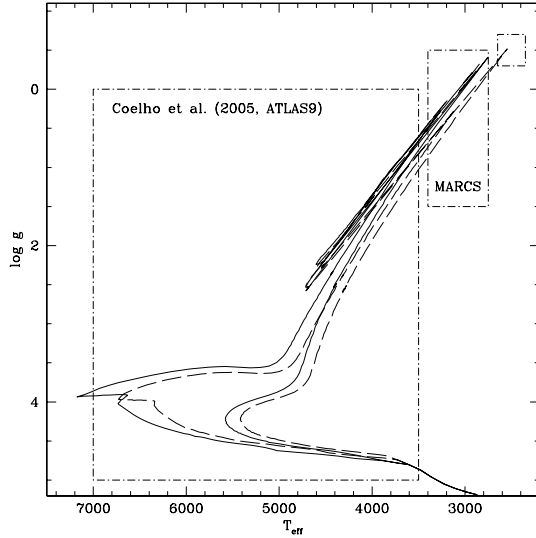
Figure 5. Isochrones of 3 and 14 Gyr at fixed [Fe/H] = 0 are shown in T_{eff} versus log g parameter space. Mixtures [α/Fe] = 0 and 0.4 are indicated as solid and dashed lines, respectively. The large dot–dashed area shows the coverage of the original stellar library by C05 (based on ATLAS9 models), and the two smaller dot–dashed areas show the extension computed in the present work (based on MARCS models).

models were computed to cover very cool giants, and smooth flux corrections were applied in order to improve the spectrophotometric predictions.

The extension to cool giants and the flux corrections are described in detail below.

3.1 Extension to cool giants

C05 library covers from 3500 to 7000 K in stellar effective temperature. The lower limit is set by the ATLAS9 model atmospheres, used as input in the spectral calculations. But it is well known that the RGB extends toward cooler stars, and these luminous giants have an important contribution to the integrated light of old stellar populations. Therefore, an additional set of synthetic spectra was computed employing the Plez (1992) MARCS models, for giants with temperatures down to 2800 K, and adopting the same atomic and molecular line list and line formation code by C05.

These MARCS models atmospheres do not account for α-enhanced mixtures in the opacities, nevertheless the α-enhanced atomic and molecular abundances were properly included in the calculation of the high-resolution spectra. We performed a test with a T_{eff} = 3500 K giant star from the ATLAS9 model atmospheres grid and we verified that this inconsistency has a negligible effect in the spectral line profiles, as long as the difference between the opacities of the model atmosphere and of the synthetic spectra is smaller then ∼0.4 dex. We also verified that the transition between ATLAS9-based spectra and MARCS-based spectra is smooth.

The coverage of the new stellar library is illustrated in Fig. 5 in the T_{eff} versus log g plane. The effect of the inclusion of the very cool giants in the integrated spectra of a 9-Gyr-old SSP model is shown in Fig. 6.

3.2 Flux corrections

Another update made to the original synthetic library concerns its spectrophotometry. A synthetic library that is intended to reproduce high-resolution line profiles with accuracy is not a library that also
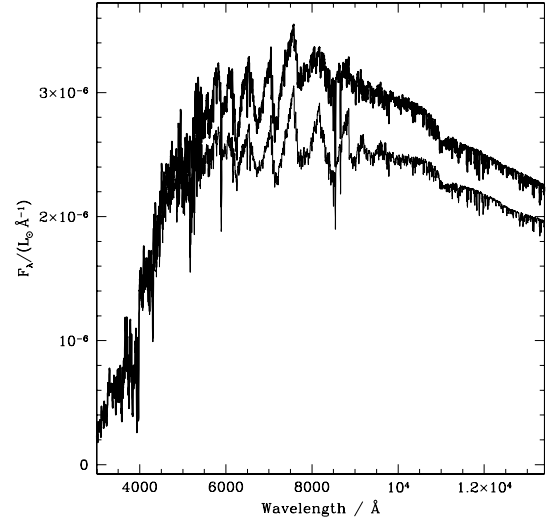

Figure 6. SED of a 9-Gyr-old SSP computed with and without the extension to cooler giants modelled for the present work (thin and thick lines, respectively).

predicts good spectrophotometry. That happens because when computing a synthetic spectrum, one has to choose to include or not the so-called 'predicted lines' (hereafter PLs, Kurucz 1992). The PLs are absorption lines for which one or both energy levels have to be predicted from quantum mechanics calculations. They are an essential contribution to the total line blanketing in model atmospheres and to spectrophotometric modelling. But as the quantum mechanics predictions are accurate to only a few per cent, wavelengths and computed intensities for these lines may be largely uncertain, and the PLs may not correspond in position and intensity to the observable counterparts (Bell, Paltoglou & Tripicco 1994; Castelli & Kurucz 2004). Therefore they are usually not included in high-resolution spectral computations focused on spectroscopic use, which is the case of the C05 library.

As a consequence, the colour predictions by C05 are inaccurate, in particular in the blue part of the spectrum. The grid by ATLAS9 provides flux distributions predictions that include all the blanketing (i.e. the PLs). In order to correct the spectra by C05, each star in this library was compared to its counterpart flux distribution by ATLAS9. Both distributions were smoothed until no spectral feature remained. The ratio of the two curves describes how the C05 synthetic star deviates from a model that includes all blanketing. This *response* was multiplied to the original spectrum given by C05, star by star. Therefore, the final spectrum kept the high-resolution features of the original C05 library, but presents a flux distribution which is closer to that predicted when including all blanketing. An original and corrected spectrum for a Sun-like star is shown in Fig. 7, in order to illustrate the effect of this correction.

4 POPULATION SYNTHESIS MODELS

The set of evolutionary tracks described in Section 2 do not follow the evolution of the stars to the last evolutionary phase for all masses. Therefore, the post-RGB evolution of the stars up to the end of the early AGB were extended by using appropriate tracks by Pietrinferni et al. (2006, hereafter BaSTI). (We are grateful to S.
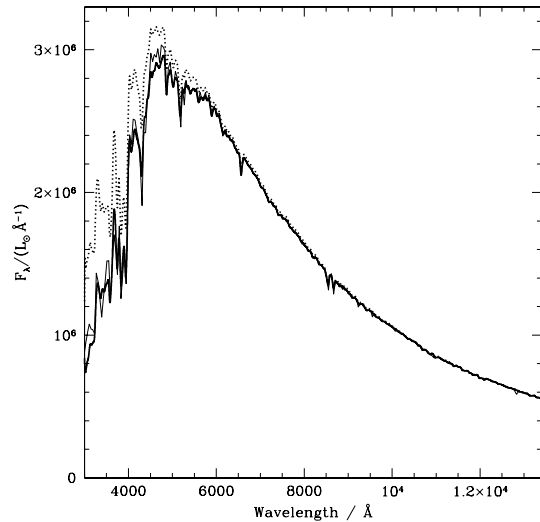
Figure 7. SED of a star with $T_{\rm eff} = 5750\,{\rm K}$, $\log g = 4.5$, [Fe/H] = 0.0 and [α/Fe] = 0.0. The thin solid line shows the flux distribution as calculated by ATLAS9. The dotted line shows the corresponding spectrum in the original C05 library (the high-resolution spectra were smoothed to the resolution of the ATLAS9 flux distributions). The thick solid line shows the spectrum adopted here, derived from the first two spectra as described in the text.

Cassisi for providing us with a set of tracks tailored to our needs.)[6] As the effective temperatures of both track sources to not agree completely along the giant branches, a smooth switching from our to the Basti tracks over one brightness magnitude was done. The temperature differences to be bridged were typically around 100 K. The calculations by Marigo & Girardi (2007) were additionally used to describe the thermally pulsing phase of the AGB (TP-AGB). The Basti and Marigo & Girardi (2007) tracks are not available for the exact mixtures in Table 1, and we used instead the tracks with the closest value of Z.

The tracks were resampled to identify the same equivalent physical stages required by the isochrone synthesis technique as implemented by Charlot & Bruzual (in preparation) (hereafter CB07). The resampled tracks include 275 steps, distributed as follows: 55 along the MS, 25 in the subgiant branch (SGB), 100 in the RGB, 55 in the horizontal branch (HB), 25 along the AGB and 15 in the TP-AGB.

By linear interpolation in the $(\log L, \log T_{\rm eff})$ plane we built isochrones describing the locus in the HRD occupied by stars of each of the six mixtures in Table 1 at ages from 3 to 14 Gyr in 1-Gyr steps. The number of stars at each of the 275 evolutionary stages included in each isochrone is computed from the initial mass function (IMF). The spectrum of the star at each position was obtained by bilinear interpolation in $(\log T_{\rm eff}, \log g)$ in the corresponding metallicity plane in the C05 synthetic stellar library, and then scaled according to the star surface area. The integrated spectrum of the stellar population follows by adding the stellar spectrum weighted by the number of stars at each position in the HRD. Our final SSP models provide the integrated spectrum of the population at 11 time-steps, in the wavelength range from 3000 Å to 1.34 μm with a constant resolution of FWHM = 1 Å (at 0.2 Å pix^{-1}).

We provide two versions of the models. The *consistent* models include only the evolutionary phases MS, SGB and RGB. In this
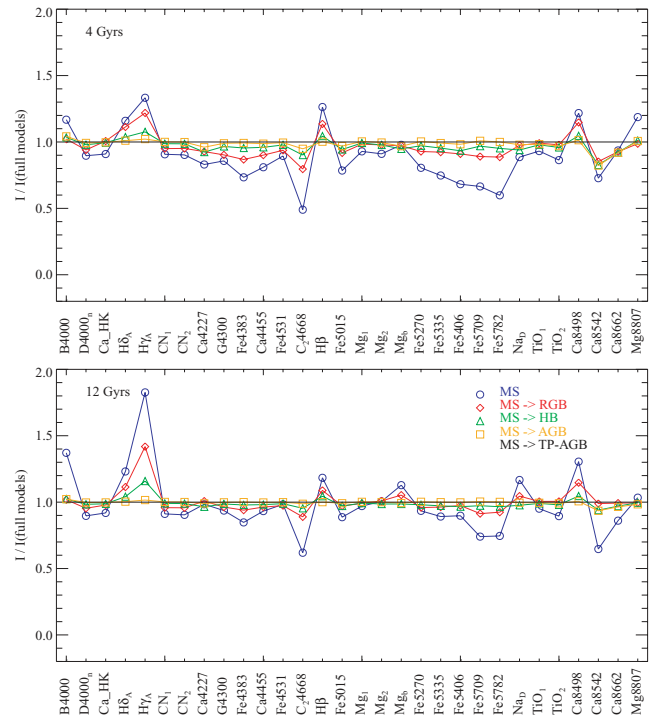
Figure 8. Lick-index strengths of model SSPs including different sets of stellar evolutionary phases (as indicated), in units of the index strengths of a model SSP including all phases (from MS to TP-AGB). The spectral indices are ordered in function of increasing central wavelength. The top and bottom panels show the results for 4- and 12-Gyr-old populations, respectively. All models have solar abundances ([Fe/H]= [α/Fe] = 0).

case, the assumptions for the chemical mixtures are fully consistent among the ingredients, and these are the preferred models to evaluate the differential effect of the α enhancement on spectroscopic and photometric observables. The *full* models include the evolutionary phases MS, SGB, RGB, HB, AGB and TP-AGB, and are more suitable to the direct comparison to observations. The effect of different evolutionary phases on the spectral indices is illustrated in Fig. 8.

We noted that the addition of the TP-AGB phase has a small effect on the *I*-band flux, affecting therefore some visual colours, as can be seen in Fig. 9. This effect is mostly seen in the younger ages and solar-scaled mixtures (the α-enhanced populations are in comparison more populated with cool stars, and the addition of a very cool TP-AGB spectrum is less significant). We consider these results as preliminary indications only, for the following reasons. The stellar spectra that represent the TP-AGB phase are selected among the MARCS-based spectra (cf. Section 3.1), which are not appropriate models to represent TP-AGB stars (that are known to be either carbon or oxygen enriched). Secondly, the effective temperatures of AGB stars are uncertain due to several uncertainties in the stellar evolution models, most notably convection in the highly superadiabatic outer envelope, structure and radiation transport in the atmosphere, and finally the composition, influenced by dredge-up and hot bottom burning, itself. Thirdly, the mass-loss, depending itself on these effects, leads to circumstellar (dust) shells, which absorb shorter wavelength light and reemits it in the far-infrared (far-IR). The properties of the circumstellar shell again depend on chemistry and mass-loss history. Several studies, among them Piovan, Tantalo & Chiosi (2003) and Groenewegen (2006) have modelled that effect in the IR, and we expect therefore that, due to the dense
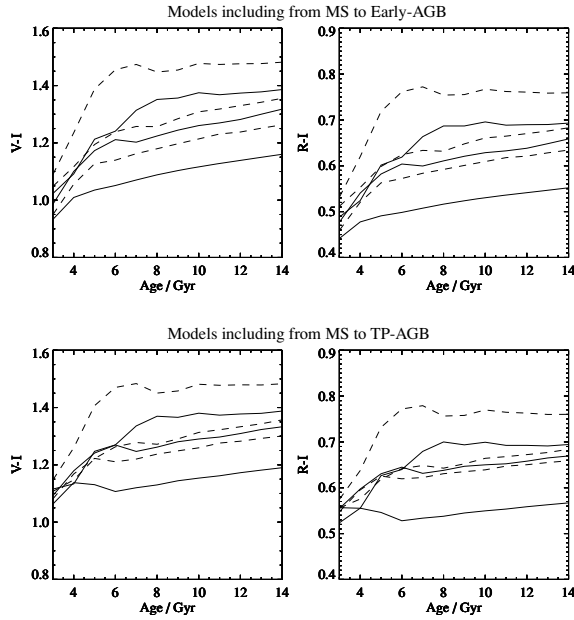
Figure 9. Colour evolution predicted by our SSP models, with and without the inclusion of the TP-AGB phase. The solid lines show the evolution of the three solar-scaled mixtures, and the dashed lines show the α-enhanced mixtures. In each case the three iron abundances are represented ([Fe/H] = $-0.5, 0.0$ and 0.2), and higher iron abundances correspond to redder colours.

circumstellar dust shells, the contribution of AGB stars to the visual and red bands will be smaller than our models indicate, but larger in the mid- to far-IR bands, where dust re-emits the absorbed radiation.

5 THE PERFORMANCE OF FULLY SYNTHETIC SPECTRAL ENERGY DISTRIBUTIONS

The major concern of using a synthetic stellar library as ingredient for SSP models regards the accuracy of the model stars when compared to observed ones. For this reason, the large majority of SSP models to date employ empirical stellar libraries. In order to assess the impact of using a synthetic stellar library on SSP models, we performed some comparisons between fully theoretical SSP models and models from literature that use empirical libraries (a detailed comparison between theoretical and empirical libraries in a star by star basis is given in Martins & Coelho 2007). It is worth noting that empirical libraries are not error-free, being affected by uncertainties on the stellar atmospheric parameters, spectrophotometric calibration issues, poorly constrained chemical pattern, telluric contamination and other effects difficult to control. We aim here at highlighting the major differences, rather than performing a definitive evaluation of the quality of the synthetic library.

5.1 Comparisons of spectral energy distributions

We computed SSP models (hereafter SYN models) with the synthetic spectral library described in Section 3 and compared them with models by BC03, which employ the STELIB (Le Borgne et al. 2003) library, and models by CB07 built with the Indo-US library (Valdes et al. 2004). In order to isolate the influence of the stellar spectral library alone, all models considered in this section employ the isochrones by Girardi et al. (2002) and a Salpeter (1955) IMF.
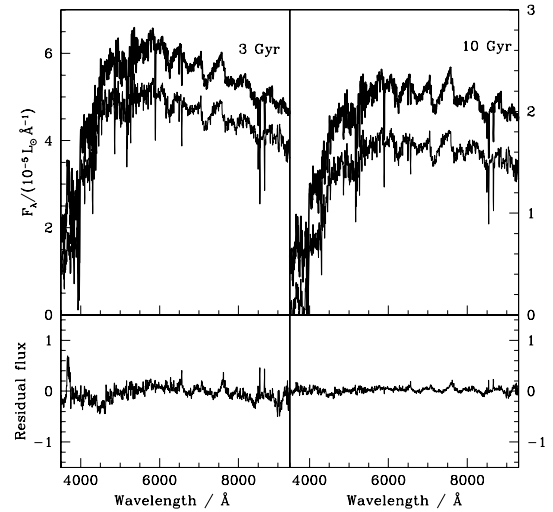

Figure 10. Top: Comparison of SSP models computed using the library of synthetic stellar spectra described in Section 3 (SYN models; thick lines) and BC03 models (thin lines), at the ages of 3 Gyr (left-hand panel) and 10 Gyr (right-hand panel). The BC03 spectra were arbitrarily shifted to facilitate visualization. Bottom: Residuals between the two models. All models were computed with the solar isochrone by Girardi et al. (2000) and a Salpeter IMF.
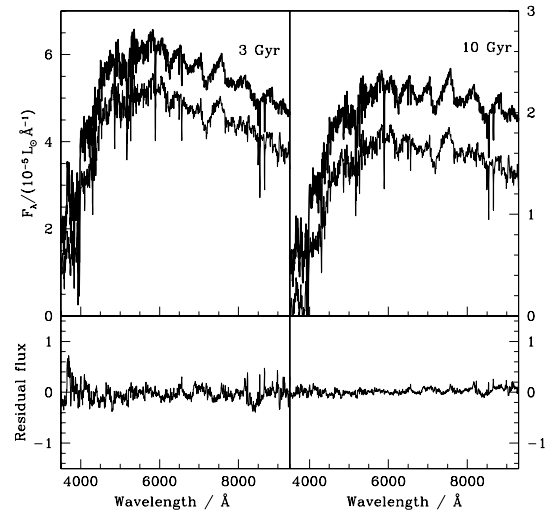

Figure 11. Same as in Fig. 10, but showing models by CB07 using the Indo-US library as thin solid lines.

The model SEDs are shown in Figs 10 and 11, comparing SYN models to the ones by BC03 and CB07, respectively, at the ages of 3 and 10 Gyr. In each case, the top panel shows the compared spectra and the bottom panel the residuals. Residuals are on average smaller for the old age population. In the case of the 3-Gyr populations, there is a residual peak centred around 3700 Å that is not present in the older age. It comes from the fact that C05 library includes only the first 10 Balmer lines in its spectrum, and as a consequence, the hotter stars in that library present a misfeature around 3700 Å due to missing higher order Balmer lines. There are also peaks at longer wavelengths (from 6500 Å on) that are related to small mismatches in the intensity of the TiO bands. From the theoretical point of view, the spectrum of this complex molecule is difficult to model, and C05 did a careful empirical calibration of the intensity
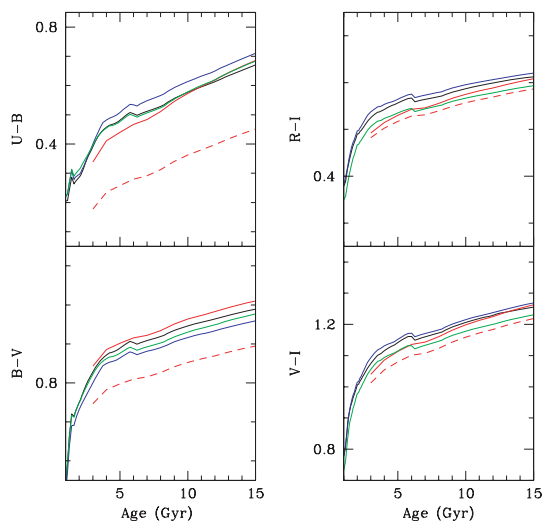
Figure 12. Colour evolution of SSPs adopting different stellar libraries. Models using empirical libraries are shown in black (STELIB) and blue (Indo-US). In green is shown the predictions by the BaSeL low-resolution synthetic library. Red solid lines are SYN models of the present work. The dashed red lines indicate models computed with the original C05 library, i.e. prior to the flux corrections explained in Section 3.2.

of the TiO bands against cool giants. From the point of view of the empirical library, this is a region dominated by cool giants, whose atmospheric parameters are largely uncertain. Also, TiO intensity is very sensitive to Ti and O abundances, and the observed stars from the solar neighbourhood may show variations on [Ti/Fe] and [O/Fe] (e.g. Reddy et al. 2003), while the synthetic library has fixed values, by construction.

5.2 Broad-band colours

To asses the spectrophotometric properties of the fully synthetic models, we computed broad-band colours and compared them to the predictions of BC03 and CB07 models. The results are presented in Fig. 12, showing the age evolution of the $(UBV)_{\rm Johnson}-(RI)_{\rm Cousins}$ colours given by SYN models (solid red lines), BC03 models (with STELIB library; black lines), CB07 models (with Indo-US library; blue lines), and an additional set of BC03 models using the BaSeL theoretical library (Lejeune, Cuisinier & Buser 1997, 1998; Westera et al. 2002, green lines). The dotted red lines indicate the colours obtained using the original C05 library, prior to the flux corrections described in Section 3.2. Fig. 12 shows that the flux corrections improve drastically the synthetic colours. The SYN colours seem to be in general marginally bluer than the average prediction given by empirical libraries (except in the $B-V$ colour that shows the opposite behaviour), but the differences are small. We conclude that the modified version of C05 library is fairly accurate in predicting broad-band colours, showing no large differences compared to models based on empirical libraries.

5.3 Classical spectral indices

To assess the accuracy of the synthetic library in predicting some of the widely used spectral indices, we measured a group of 30 indices on SYN models. These indices were compared to the predictions by BC03, CB07 (with Indo-US library), Vazdekis et al.

Table 2. Observational errors adopted in Fig. 13.

Index	Observational error
B4000	0.062
$D_n(4000)$	0.054
Ca H&K	0.040
$H\delta_A$	0.942
$H\gamma_A$	0.908
CN_1	0.027
CN_2	0.908
Ca4227	0.452
G4300	0.809
Fe4383	1.063
Ca4455	0.506
Fe4531	0.816
C4668	1.286
$H\beta$	0.524
Fe5015	1.275
Mg_1	0.016
Mg_2	0.021
Mg b	0.653
Fe5270	0.673
Fe5335	0.690
Fe5406	0.535
Fe5709	0.376
Fe5782	0.336
Na D	0.460
TiO_1	0.012
TiO_2	0.010
Ca8498	0.162
Ca8542	0.156
Ca8662	0.179
Mg8807	0.129

(2003)[7] and Vazdekis et al. (in preparation)[8] models. The selected indices encompass the classical Lick/IDS indices as defined by Trager et al. (1998), the higher order Balmer lines by Worthey & Ottaviani (1997), the near-IR indices by Diaz et al. (1989), two definitions of the D4000 break (Bruzual 1983; Balogh et al. 1999) and the blue Ca H&K index by Brodie & Hanes (1986). All models were smoothed to a common resolution of 70 km s^{-1} prior to the measurement of the indices. The results are shown in Fig. 13, which shows the differences of model indices relative to Indo-US models by CB07, in units of the observational errors. The observational errors are taken from red galaxies in SDSS-DR4 with S/N $\geqslant$ 40 per pixel, and are listed in Table 2. For most of the indices the agreement is very good. The larger discrepancies are discussed below.

Balmer line indices: All the Balmer indices are underestimated in the SYN models. This effect was expected because it is known that Hydrogen lines computed in local thermodynamic equilibrium (LTE) match well the wings, but cannot reproduce the core of the lines. Better suited microturbulence velocities and/or a mixing length to pressure scaleheight ratio $\ell/H_{\rm p}$ improve somewhat the match (e.g. Canuto & Mazzitelli 1992; Fuhrmann, Axer & Gehren 1993; van't Veer-Menneret & Megessier 1996; Bernkopf 1998; Barklem et al. 2002), and this is the reason why Barbuy et al. (2003) recomputed the ATLAS9 model atmospheres with $\ell/H_{\rm p} = 0.5$, but a single value is hardly sufficient for all spectral types.

---

[7] These models are based on Cenarro et al. (2002) stellar fitting functions and cover the near-IR wavelength range.
[8] Based on the recent MILES library by Sánchez-Blázquez et al. (2006), Cenarro et al. (2007), covering the optical wavelength range.
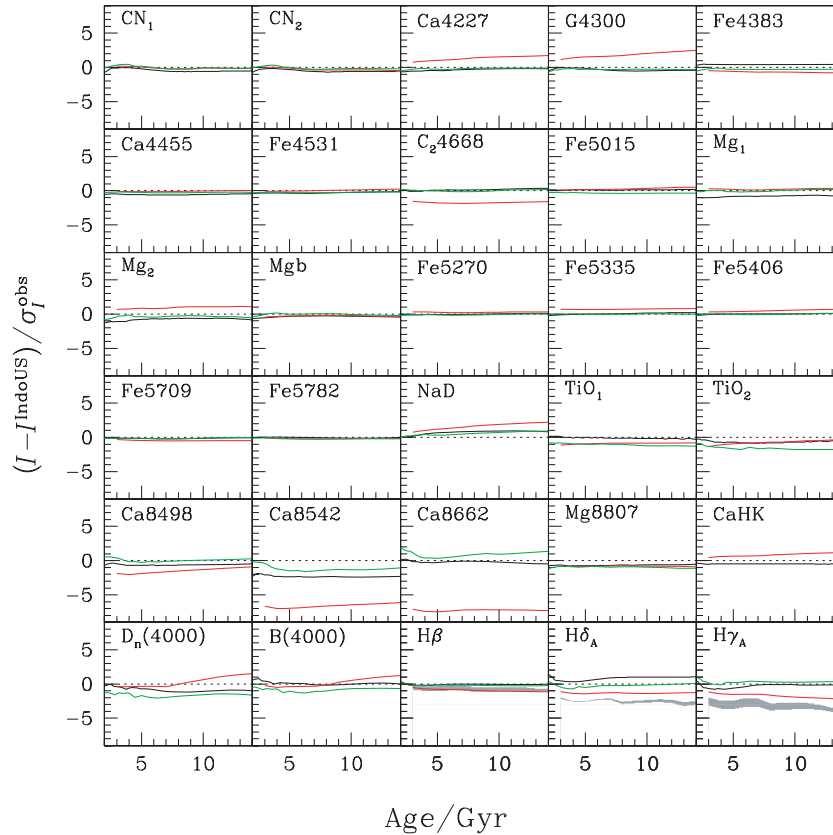
Figure 13. Evolution of spectral indices, for SSP models computed using different stellar libraries. BC03 models are shown in black, SYN models in red and Vazdekis models (built with either MILES or Cenarro et al. 2002 libraries) in green. For each index, the *y*-axis shows the difference between a given SSP model and the CB07 Indo-US model, in units of the typical observation error (Table 2). In the panels that show Balmer line indices, the shaded region shows the values predicted by other two high-resolution theoretical libraries (Martins et al. 2005; Munari et al. 2005).

Besides, the bottom of the hydrogen lines form in the chromosphere, not included in the model atmospheres. In the very cool stars these lines are weak and have essentially no wings, and as a consequence the indices are dominated by a non-satisfactory line core modelling. We built models based on two other recent synthetic libraries (Martins et al. 2005; Munari et al. 2005 shown as a shaded region in fig. 13), and we confirm that these stellar models show the same systematic behaviour.

Indices sensitive to C and N abundances: Among the indices sensitive to C and/or N abundances, G4300 and $C_2$4668 deviate more than 3σ from the predictions based on empirical libraries. We believe this happens partially because in C05 library, the C and N abundances relative to Fe were assumed to be solar through all evolutionary phases. But it is well known that the CNO cycle lowers the C abundance and enhances the N abundance in giants (e.g. Iben 1967; Charbonnel 1994). The same effect on the indices CN_1 and CN_2 would not be so clearly seen because in these indices the variations of C and N somewhat compensate each other. The calculation of a subgrid of the synthetic models accounting for C and N abundance variations is underway and will be presented in a separate paper (with similar assumptions to the ones adopted in Barbuy et al. 2003, and additionally including consistent computations for the model atmospheres). It is interesting to note that another index that deviates by similar amounts is Ca4227. Despite its designation, the Tripicco & Bell (1995) tables show that the sensitivity of this index to C variations is of the same order as its sensitivity to Ca abundance variations.

Near-IR Ca indices: The near-IR indices show the biggest deviation among all the indices (Ca8542 and Ca8662 deviate beyond 5σ in error units). When we compared the C05 calculations with very high-resolution observed spectra of the Sun and Arcturus (Kurucz et al. 1984; Hinkle et al. 2000), we found that the synthetic indices were underestimated (as expected from the lack of N-LTE line profile calculation, see e.g. Cayrel et al. 1996), but the differences were typically three times smaller than the difference shown in Fig. 13. The larger difference found in the SSP models is possibly coming from a source different than only inaccuracies in the synthetic stars. We noted that Bensby et al. (2005) found that the disc stars with [Fe/H] = 0.0 ± 0.1 tend to have [Ca/Fe] values in the range between 0.0 and 0.1, so it is possible that models built with empirical libraries are contaminated by stars with [Ca/Fe] $\neq$ 0.0, that would prevent a proper match by SYN models.[9] This effect would not be so clearly seen in the blue Ca indices because the response of the red Ca indices to [Ca/Fe] is considerably stronger (see Appendix A in the Supplementary Material, available only in the online version of this paper). Additionally, this wavelength range is dominated by cool giants, whose stellar parameters in the empirical libraries are largely uncertain, and Martins & Coelho (2007) show that these indices are also highly sensitive to flux-calibration issues. We conclude that the large discrepancy is related both to uncertainties in the

---

[9] The solar models by BC03 include stars from STELIB with $-0.06 \leqslant$ [Fe/H] $\leqslant +0.07$. CB07 models adopt the range $-0.10 \leqslant$ [Fe/H] $\leqslant +0.10$.
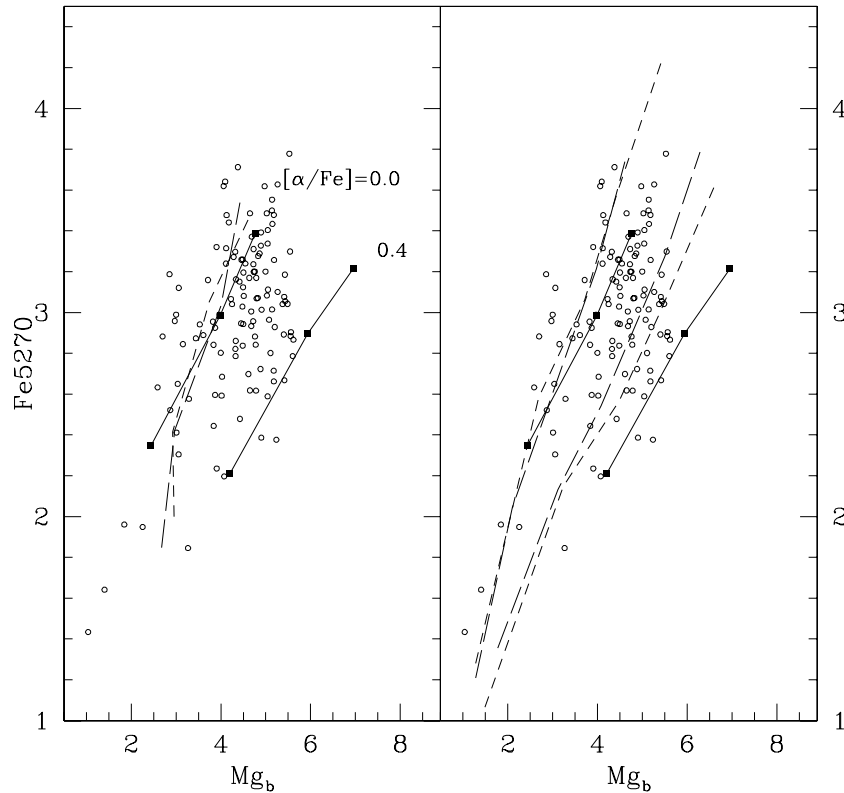
Figure 14. SSP models at constant age of 12 Gyr are plotted with the galaxy data from Trager et al. (1998). Left-hand panel: Solid lines show models by the present work, where the solid squares indicate [Fe/H] = −0.5, 0.0 and 0.2 (the most metal-rich systems have higher index values). Short-dashed lines indicate BC03 models, and long-dashed lines are CB07 Indo-US models. Right-hand panel: The solid line is the same as in the left-hand panel. Short-dashed lines are models by Thomas et al. (2003b), also for [α/Fe] 0.0 and 0.4. Long-dashed lines indicate models by Schiavon (2007).

synthetic calculations (due to N-LTE effects) and uncertainties in the empirical libraries (abundance pattern, atmospheric parameters and flux-calibration issues).

6 MODEL PREDICTIONS

In this section we present the new spectral models, computed with the ingredients described in Sections 2 and 3, the synthesis code presented in Section 4 and adopting IMF by Chabrier (2003). The space parameter covered by the models is summarized below:

(i) wavelength range: from 3000 Å to 1.34 μm;
(ii) [Fe/H]: −0.5, 0.0 and 0.2;
(iii) [α/Fe]: 0.0 and 0.4;
(iv) total metallicity Z: 0.005, 0.011, 0.017, 0.026, 0.032, 0.048;
(v) ages: 3–14 Gyr (1-Gyr step).

The original resolution of the models is FWHM = 1 Å with a sampling of 0.2 Å pix^{-1}, and we provide additionally models convolved to the wavelength-dependent instrumental resolution of SDSS. Different resolutions and samplings can be obtained by appropriately convolving the original models.

Some applications of the models are presented below.

6.1 Classical Mg versus Fe plot

The best known result that illustrates the effects of α enhancement on spectral properties of galaxies are those of magnesium versus iron indices (e.g. Worthey et al. 1992), where solar-scaled

models cannot reproduce the locus of high-mass spheroidal galaxies. In Fig. 14 we present our models for 12-Gyr populations (solid lines) in the Fe5270 versus Mg b plane, with galaxies from Trager et al. (1998) sample, which span a large range in masses.

The indices were measured at the Lick/IDS resolution as tabulated in Worthey & Ottaviani (1997). The synthetic stellar library employed in our models is closer to a flux-calibrated system than to the Lick/IDS flux system. We translated our measurements to the standard Lick/IDS adopting the zero-point corrections tabulated in BC03 (which translates the flux calibrated stellar library STELIB to the Lick/IDS system).

In the left-hand panel of Fig. 14, the short- and long-dashed lines are the predictions given by BC03 and CB07 models, respectively. It can be seen that the present models successfully cover the gap left by previous spectral models, i.e. by producing models that fill the locus of the massive early-type systems.

In the right-hand panel we show the models of the present work and the Lick/IDS model indices by Schiavon (2007) (short-dashed lines) and Thomas et al. (2003b, long-dashed lines), so that we can see how our models compare with Lick/IDS models available in the literature. The behaviour of all α-enhanced models shown in Fig. 14 is similar, in the sense that the α-enhanced models have stronger Mg indices when compared to iron indices. In detail, our models tend to produce stronger Mg indices at the same adopted mixture of [α/Fe] = 0.4.

Besides the different ingredients and methodologies, there is a particular difference in our approach of accounting for the α enhancement, with respect to the ones available in literature, that is
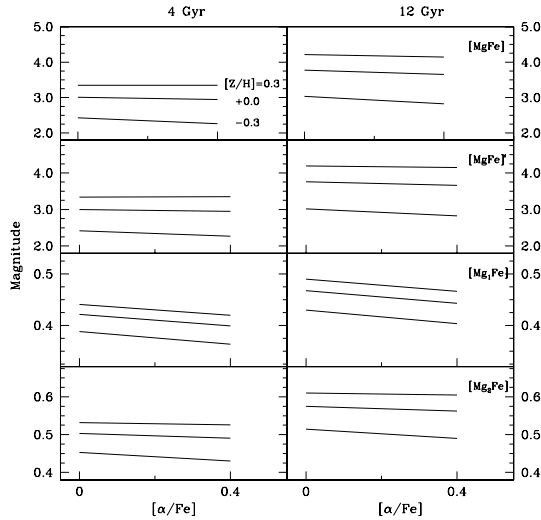
Figure 15. The behaviour of four indices defined to be insensitive to [α/Fe], given by González (1993), Thomas et al. (2003b) and BC03. The behaviour for two ages and three different values of [Z/H] were inspected. The models for 4 Gyr are shown in the left-hand panel and models for 12 Gyr are shown in the right-hand panel. Each row shows the behaviour of an index, as indicated in the top right-hand corner of each panel. The three lines in each panel correspond to [Z/H] = −0.3, 0.0 and 0.3, from bottom to top.

worth highlighting. Lick/IDS model indices (like those of Thomas et al. 2003b; Schiavon 2007) use the response functions to include the different abundance patterns. When deriving the response functions (Tripicco & Bell 1995; Houdashelt et al. 2002; Korn et al. 2005), the calculations of synthetic spectra consider *individual* element enhancements, whereas other work (e.g. Barbuy et al. 2003; ATLAS9; Gustafsson et al. 2003; C05; Munari et al. 2005; Brott & Hauschildt 2005), as well as the present models, assume *all* α elements enhanced together. It is not clear if the effect of enhancing all α elements is equivalent to a linear combination of the effects due to individual abundance variations. That is because in stars of spectral type G to M, the continuum forms mainly by free–free and bound–free transitions of H^-. The amount of H^- present depends on the electrons captured by Hydrogen atoms, coming in good part from α elements that are important electron donors. Therefore one of the main effects of α-element enhancement is a lowering of the continuum, and a clear example is the weakening of the Fe5270 and Fe5335 indices in spectra with α-element enhancements, at fixed iron abundances (e.g. Barbuy et al. 2003). In fact all the spectrum gets weaker from the lowering of the continuum, whereas atomic and molecular lines involving α elements get stronger due to the higher abundance. In some cases, like that of the Mg_2 index, the stronger intensity of the Mg I + MgH lines present in the Mg_2 region overcome the lowering of the continuum, and the index becomes stronger with α enhancement (e.g. Barbuy 1994). Therefore, it seems to us that an overall enhancement of the α-element abundances can have an impact on the continuum (and therefore in the indices) that is different from combining the impact of varying the abundance of each element individually, through the response functions.

6.2 Indices insensitive to α/Fe

Indices defined to be insensitive to α/Fe, providing a good measurement of the total metallicity, have been used frequently in the literature. Most of the SSP models available in literature adopt a *fixed Z* approach, as proposed by Trager et al. (2000) (the total metallicity

Z is the same for the solar-scaled and for the α-enhanced model). In order to keep the total metallicity constant, the iron abundance of the α-enhanced models has to be lowered (*iron depletion*). The present models, being computed at fixed [Fe/H], do not directly provide predictions at fixed *Z*. For the purpose of exploring some of the total metallicity indicators, we interpolated a small set of our models to estimate indices for three values of [Z/H] (−0.3, 0.0, +0.3) and two ages (4 and 12 Gyr). We studied four indices: [MgFe] as given by González (1993), [MgFe]′ by Thomas et al. (2003b) and [Mg_1Fe] and [Mg_2Fe] by BC03; and the results are shown in Fig. 15. We find that the [Mg_1Fe] index gets smaller with increasing [α/Fe], for any age or *Z* calculated. For the three remaining indices, [MgFe], [MgFe]′ and [Mg_2Fe], we confirm that they are fairly insensitive to α/Fe. There is a hint that at subsolar values of *Z* there is some dependence with α/Fe, but it is rather small. We see no appreciable difference among the behaviour of these three indices.

6.3 Effect on colours

For the first time we can explore the effect of the α enhancement on the broad-band colours of SSPs. In Fig. 16 is shown the evolution of the SSP colours as a function of age, from the *consistent* models of the present work. Solar-scaled models are shown as thin black lines and α-enhanced models are shown in red thick lines. Iron abundances from bottom to top are [Fe/H] = −0.5, 0.0 and 0.2. We can see that for the bluest colours, $U − B$, $B − V$ and $u − g$, the α-enhanced model is slightly bluer than its solar-scaled counterpart, even though the total metallicity increases. This goes in the opposite direction of what is normally expected, i.e. that more metal-rich populations are redder. Given that the α-enhanced isochrones are indeed redder than the solar-scaled ones at the same iron abundances (cf. Fig. 5), this effect is coming from the stellar energy distributions. The α enhancement changes the continuum of a high-metallicity star in a peculiar way, thus the α-enhanced models are bluer in the blue bands, and redder in the red bands than the solar-scaled models. These findings are in agreement with the work by Cassisi et al. (2004) on stellar colour transformations, and implies that the colour relations for metal rich α-enhanced populations cannot be described as rescaling of the solar-scaled ones.

6.4 Evolutionary *versus* spectral effect

With the present models we can verify if the influence of the α enhancement on spectral observables is dominated by evolution (i.e. by the α-enhanced tracks) or by stellar spectra (i.e. by the α-enhanced stars). In order to quantify each of these effects, we computed two additional set of models: the *evolution effect* is shown by models in which α-enhanced tracks were combined with the solar-scaled stars; similarly, the *spectral effect* is shown by models in which α-enhanced stars were combined with solar-scaled tracks.

Our results are presented in Figs 17 and 18, for spectral indices and broad-band colours, respectively (we also provide tables with model predictions in Appendix A in the Supplementary Material, which is available only in the online version of this paper). In each figure, the *y*-axis shows the difference between the *alpha*-enhanced prediction and the solar-scaled one, in units of the solar-scaled value, while the *x*-axis shows the observables, in order of increasing wavelength. We present the results for each [Fe/H] of our models (in rows), and for ages 4 and 12 Gyr (in columns). The green and red lines correspond to the evolutionary effect and spectral effects, respectively. The black lines are the predictions in which both effects are considered, given by the *consistent* models.
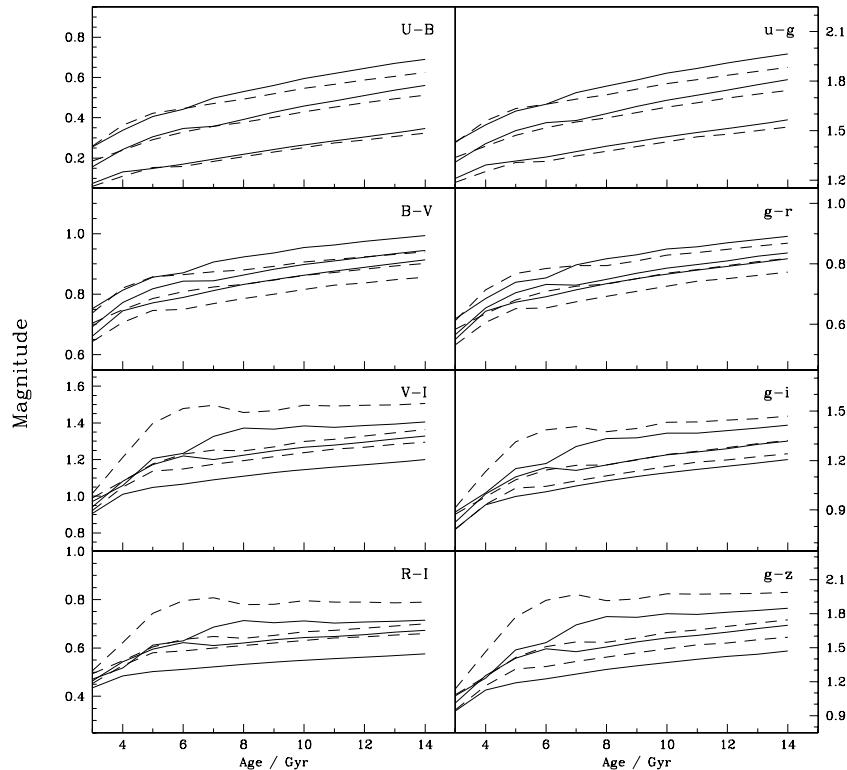
Figure 16. The colour evolution predicted by the *consistent* models, as described in Section 4. The colours are indicated in each panel: the left-hand panels show the colours in Johnson–Cousins system, and the right-hand panels show the SDSS colours. The solid lines are the solar-scaled models and the dashed lines are α-enhanced models. The [Fe/H] increases from bottom to top and has values −0.5, 0.0 and 0.2.

In Fig. 17 we see that most of the indices are dominated by spectral effects. Nevertheless there are cases where the evolutionary effect is non-negligible, namely the Balmer lines. In general indices at longer wavelengths than Fe5782 are more sensitive to evolution effects. In the case of colours (Fig. 18), both effects are often equally important. We note in particular how the spectral effect tends to lower the $U − B$ values, while the evolution effect tends to increase them. These results highlight the importance of a consistent modelling of both ingredients.

6.5 Comparison with Sloan elliptical galaxies

In order to further compare our models with observations, we selected galaxies from the SDSS-DR4 with velocity dispersions between 250 and 300 km s^{-1}, and concentration parameter $c >$ 2.8. Thus our sample is dominated by massive early-type galaxies [there might be some contamination by non-elliptical galaxies, but it should be small (see e.g. Gallazzi et al. 2005)]. Only spectra with S/N $\geqslant$ 40 were considered. The models were convolved to the instrumental resolution of the SDSS spectrograph, and then broadened to a velocity dispersion of 275 km s^{-1}. We compare our models to these observations in *index versus index* plots, shown in Figs 19 to 22. Models for 12 Gyr are shown as solid lines grid, and models for 3 Gyr are shown as dashed lines. The grid lines connect models at fixed [α/Fe] (0.0 and 0.4) and at fixed [Fe/H] (−0.5, 0.0, 0.2).

The Balmer indices: Fig. 19 presents the Balmer indices versus an index sensitive to Mg (Mg b, left-hand column of the figure) and an index sensitive to Fe (Fe5270, right-hand column). No attempt was made in calibrating the models, due to the uncertainties that affect the synthetic Balmer lines (cf. explained in Section 5.3), and

we expected some systematic deviations, but in overall the models reproduce very well the observations. Our models show that Hδ_A and Hγ_A are more sensitive to α enhancement than Hβ, confirming the findings by Thomas, Maraston & Korn (2004) from an independent method.

Iron sensitive indices, Na D and TiO: In Fig. 20 we present the indices that are highly sensitive to iron abundance, besides Na D and TiO, as a function of Mg b. All the indices sensitive to Fe are very well reproduced, even though we note that the bluest index, Fe4383, tend to concentrate around models with lower [α/Fe] than the other Fe indices. We note from Tripicco & Bell (1995) work that this index is more sensitive to C and Ca abundances, which might explain the slightly different behaviour. The modelled Na D is weaker than the indices observed in the elliptical galaxies. There is strong observational evidence in the literature that Na is enhanced in ellipticals (e.g. Worthey 1998). Besides, the recent work by Lecureur et al. (2007) found a significant overabundance of Na/Fe in bulge stars of our Galaxy, which supports the same findings for ellipticals (given that it is reasonable to assume that our bulge and elliptical galaxies share a similar star formation history). Regarding the TiO indices, particularly difficult to model and extremely sensitive to the temperature of the giant branch, it is very reassuring that the general locus of the models coincides well with the galaxies.

Indices sensitive to C an N abundances: Fig. 21 presents all the indices that are known to depend either on C or N abundances, or both. Despite their names, Ca4227 and Mg$_1$ were also included in this figure. because the index Ca4227 has a sensitivity to C variations of the same order of the sensitivity to Ca abundance variations (this is due to lines from the *G*-band CH A^{2}Δ− X^{2}Π and blue CN B^{2}Σ− X^{2}Σ). Concerning Mg$_1$, this index sensitivity to C abundances is
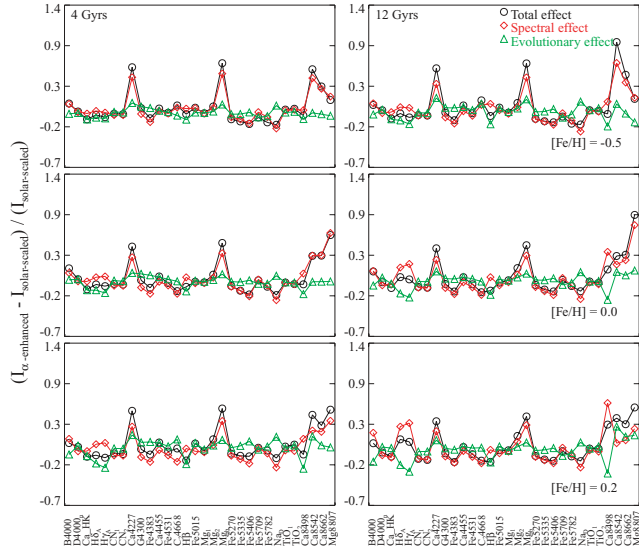
Figure 17. Differences between the α-enhanced predictions and the solar-scaled ones, in units of the solar-scaled value, for several spectral indices shown on *x*-axis. Each row corresponds to the prediction of a different [Fe/H] of our models. Left- and right-hand columns show the predictions at the ages of 4 and 12 Gyr, respectively. The green and red lines correspond to the evolutionary effect and spectral effects, respectively. The black lines are the predictions when both effects are considered together. To avoid division by zero, the scales of the three Balmer indices and Ca 8498 (which can reach negative values) were shifted arbitrarily upwards.

even larger than its sensitivity to Mg abundances [due to the $C_2(0,0)$ band head of the Swan $A^3\Pi - X^3\Pi$ system at 5165 Å]. In Fig. 21, the models are poorly representing the elliptical galaxy measurements. This is expected, because the present models do not take into account variations in the elements that dominate these indices. A modelling of C and N variations is required, considering both the CN mixing in giants (cf. explained in Section 5.3), and also non-solar primordial ratios.

Non-Lick indices: The indices that are not in Lick/IDS system are presented in Fig. 22, versus Mg *b* (left-hand column) and Fe5270 (right-hand column). In the first two rows, we show for the first time the sensitivity of the 4000 break indices with [α/Fe]. In the panels showing the 4000 break indices versus Mg *b*, we clearly see that the ellipticals concentrate over the α-enhanced models. Next in the figure we show four Ca indices (the blue Ca H&K and the three near-IR indices). The redder indices show less data points because these indices could be measured only in low-redshift galaxies. It has been claimed that ellipticals are under abundant in Ca (e.g. Thomas, Maraston & Bender 2003a), although there is still room for debate (e.g. Prochaska, Rose & Schiavon 2005). In our bulge, which is believed to be a reference population for ellipticals, high-resolution stellar spectroscopy also suggests low values of [Ca/Fe] (e.g. Zoccali et al. 2004; Alves-Brito et al. 2006), while in the metal-poor population of our Galaxy the Ca is overabundant, following the trend of the other light elements (e.g. Cayrel et al. 2004). In the present models, the Ca abundance is locked to the other α elements. The possibility of using the red Ca indices to measure the [Ca/Fe] of ellipticals is worth to be investigated, specially given the fact the blue Lick/IDS index sensitive to Ca, Ca4227, responds in non-negligible ways to C variations (see also Prochaska et al. 2005). Among the four Ca indices, Ca8542 is the one that appears to be better reproduced by the models. Ca8662 shows a large
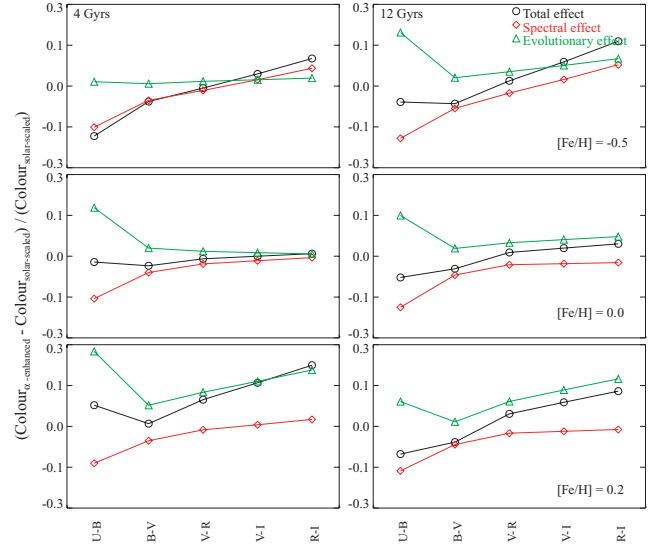

Figure 18. Differences between the α-enhanced predictions and the solar-scaled ones, in units of the solar-scaled value, for broad-band colours shown on *x*-axis. Each row corresponds to the prediction of each [Fe/H] of our models. Left- and right-hand columns show the predictions for 4 and 12 Gyr, respectively. The green and red lines correspond to the evolutionary effect and spectral effects, respectively. The black line are the predictions when both effects are considered together.

spread in the observational measurements, spreading around the mean values of the models (Ca8662 versus Mg *b* panel), and spanning the locus between the solar-scaled and the α-enhanced models (Ca8662 versus Fe5270 panel). Models for Ca8498 are too strong when compared to observations. The models for Ca H&K, the only blue alternative, are in better agreement than the Ca8498, but still marginally too strong. The galaxy measurements for the last index, Mg8807, show a large spread and no unambiguous conclusion can be reached.

7 SUMMARY AND CONCLUSIONS

We have presented a new set of fully synthetic models to compute the spectral evolution of stellar populations with solar-scaled or α-enhanced chemical compositions. These are the first models allowing one to compute the full, high-resolution spectral evolution of stellar populations with an abundance pattern different from that of the solar neighbourhood.

We focused on consistency while computing and gathering the ingredients for the models. As the first ingredient of a synthetic spectral model are the stellar tracks, we produced completely new stellar models (cf. Section 2) in a mass range of $0.6–10\,\mathrm{M}_\odot$ for six different compositions. Three of them were for solar-scaled metal ratios and three values of [Fe/H], from subsolar to supersolar. The remaining three sets had mixtures of identical [Fe/H], but with α-enhanced element ratios, such that total metallicity, helium and hydrogen abundances are different from the solar cases. The individual chemical compositions were taken into account as consistently as possible, most notably in the high- and low-temperature opacities, for which new up-to-date data were calculated. The iron abundance values and α elements ratio adopted are the same as in the synthetic stellar library.

The stellar synthetic library (cf. Section 3) is based on the one by C05, extended to cover very cool giants by computing new
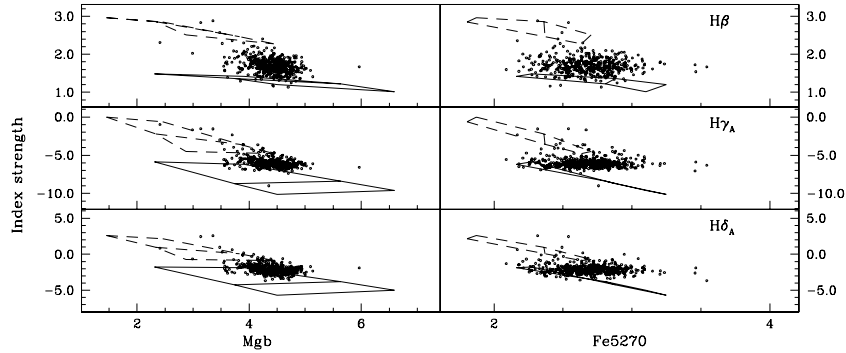
Figure 19. Three of the indices defined to measure the Balmer lines, as a function of Mg *b* and Fe5270. Solid grid lines are models at fixed age 12 Gyr, dashed lines indicate models of 3 Gyr. The models with [α/Fe] = 0.4 are represented with the right-hand side line, i.e. the ones with higher Mg *b* values. The three parallel lines connect fixed [Fe/H] values (−0.5, 0.0 and 0.2), and indices become weaker with increasing Fe abundances. Dots are massive early-type galaxies selected from the SDSS-DR4.
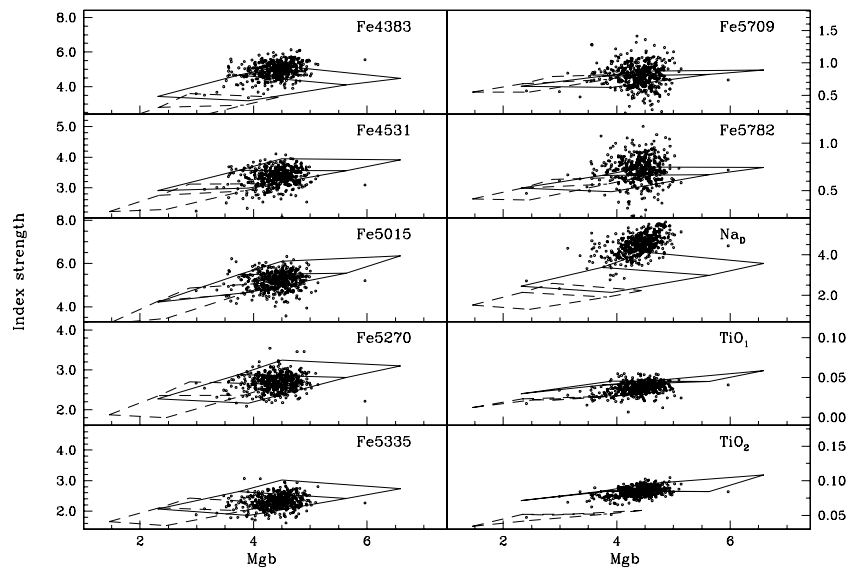

Figure 20. Indices highly sensitive to Fe abundances versus Mg *b*. TiO_1, TiO_2 and Na D are also shown here. Models are shown as explained in Fig. 19.

high-resolution spectra based on Plez (1992) model atmospheres. The photometric properties of the stellar library was significantly improved by correcting the effect of missing line opacities, through the comparison of C05 stars to the flux distributions by ATLAS9. In Section 5, the performance of the synthetic stellar library was analysed by comparing our models with models built employing empirical libraries. The results were much encouraging, with broad-band colours and most of the indices being fairly well reproduced. The exceptions are spectral indices sensitive to either C or N abundances (given that C and N abundance variations are not yet modelled) and the Balmer lines indices (due to the lack of chromosphere models and realistic N-LTE computations). The remaining differences are consistent with the uncertainties in the atmospheric parameters, abundance pattern and flux calibration of the stars in the empirical libraries.

With new tracks and an updated C05 library, we produced *consistent* SSP models that include the MS, SGB and RGB evolutionary phases (cf. Section 4). These are the most consistent models available so far that allow for evaluating the influence of α enhancement on spectral and photometric observables of stellar populations. The differential effect of the α enhancement on the several spectral and

photometric observables mentioned in this work are tabulated in Appendix A (available only in the online version of this paper). For the first time the effect of the α enhancement on broad-band colours of SSPs can be modelled, and we show that the α-enhanced colours $U − B$, $B − V$ and $u − g$ are bluer than solar-scaled ones at fixed [Fe/H], in agreement with the work by Cassisi et al. (2004) on α-enhanced colour transformations. We intend to look for an observational counterpart to test if our predictions are quantitatively correct.

In order to additionally provide a set of models that can be directly compared to observations, we extended our evolutionary tracks in a non-consistent way, by including calculations by Pietrinferni et al. (2006) (to account for the HB and early AGB) and Marigo & Girardi (2007) (to account for the TP-AGB). We show that these spectral models can reproduce the locus of ellipticals galaxies in Mg *b* versus Fe5270 plots (Section 6), where we see that our models predict slightly stronger Mg indices than previous work (Thomas et al. 2003b; Schiavon 2007), for the same value of α enhancement.

We also produced models in which we separate the influence of either the evolution or the spectra in the α-enhanced predictions. We conclude that the spectral indices are largely dominated by the
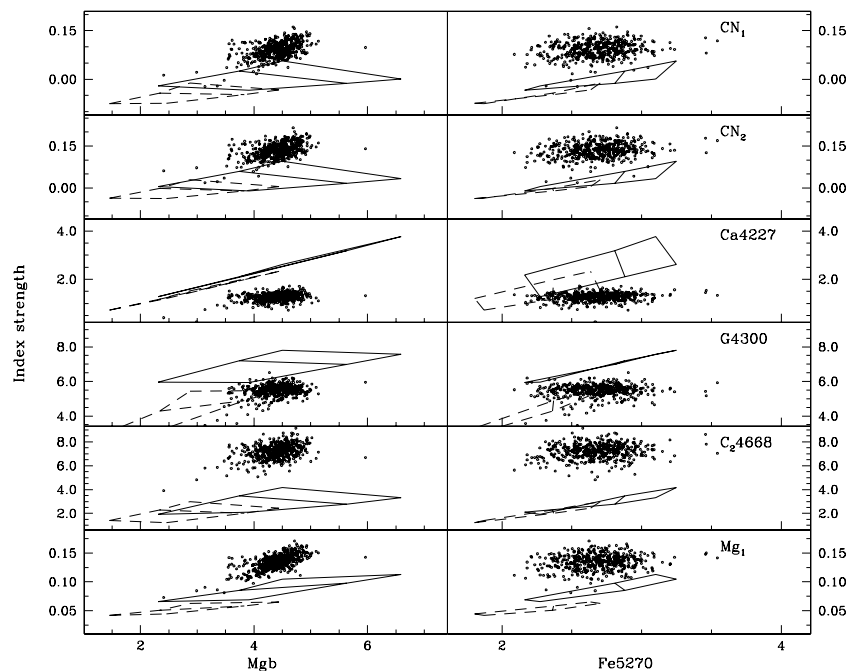
Figure 21. Indices that are known to be sensitive to either C or N abundance ratios. Models are shown as explained in Fig. 19. The α-enhanced models are the ones with higher Mg b values. The [Fe/H] values increase for stronger indices.
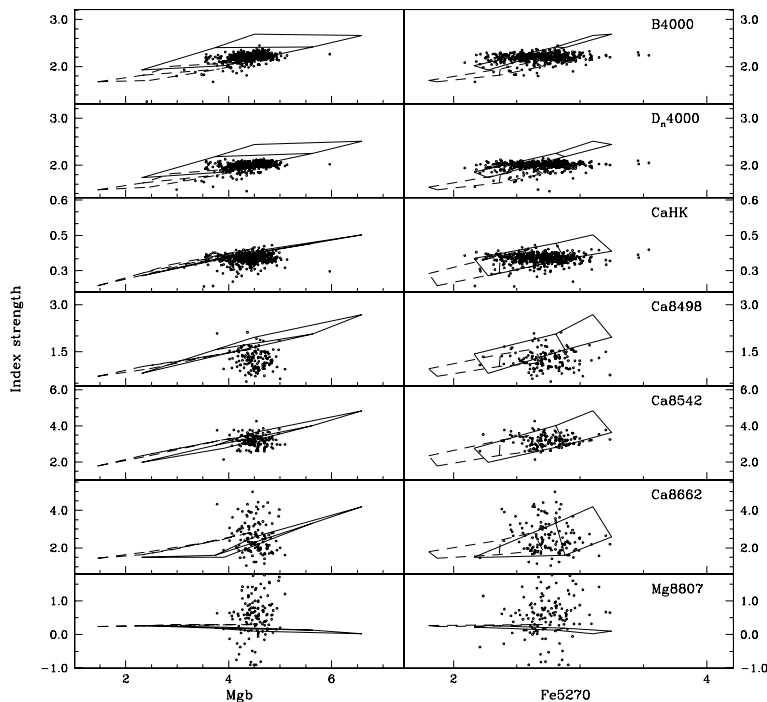

Figure 22. Non-Lick indices explored in the present work, as a function of Mg b and Fe5270 values. Models are shown as explained in Fig. 19.

spectral influence. Nevertheless the evolution has non-negligible effects on some indices, among them the Balmer lines. As for the broad-band colours, the resulting α-enhancement effect is a combination of both evolution and spectra, and thus any colour predictions should include both effects consistently.

We confirm two findings from previous work.

(i) The indices [MgFe], [MgFe]' and [Mg$_2$Fe], defined by González (1993), Thomas et al. (2003b) and BC03, respectively, are fairly insensitive to α/Fe. We do not confirm the same for the

index [Mg$_1$Fe] by BC03. No appreciable difference could be detected in the behaviour of the three 'overall metallicity' indices, for the two ages and three values of [Z/H] analysed.

(ii) The high-order Balmer indices Hδ$_A$ and Hγ$_A$ are more sensitive to α/Fe variations than Hβ, as originally shown by Thomas et al. (2004).

Lastly, we compared our spectral predictions with indices measured in elliptical galaxies observed by the SDSS-DR4. All the indices that are highly sensitive to either Fe and α elements are very well matched. The Balmer indices are believed to be somewhat underestimated, nevertheless our models reproduce reasonably well the typical values of massive ellipticals. Indices that are sensitive to C, N, Ca or Na abundances have to be further modelled before they can match observed values.

We conclude that our models are suitable for the following applications.

(i) Deriving the *response* of any observable in the wavelength region covered by the models to the overall α enhancement. These models are an alternative to employing response functions and fitting functions to model Lick/IDS indices. More important, they provide a tool to derive the sensitivity of several observables, in particular those that are not described by fitting functions, e.g. Rose (1985) indices and broad-band colours.

(ii) Deriving SSP parameters in a *differential* way. As examples, the work by Kelson et al. (2006) and Smith et al. (2006) use methods of deriving the parameters differentially, in order to avoid the systematic errors present in both models and data.

(iii) Full spectrum analysis of stellar populations (e.g. Panter, Heavens & Jimenez 2003; Cid Fernandes et al. 2005; Mathis, Charlot & Brinchmann 2006), with the caveat that regions known to have important systematic offsets when compared to empirical stellar libraries should be avoided in the analysis.

Our models open a new path for stellar population studies, by starting to fill a gap which existed among the full spectral evolution models. We plan to continuously update the models presented here, by including future upgrades and extensions of their ingredients.

The spectral models are publicly available upon request.

ACKNOWLEDGMENTS

REFERENCES

Adelberger E. G., Austin S. M., Bahcall J. N., Balantekin A. B., Bogaert G., Buchmann L., 1998, Rev. Mod. Phys., 70, 1265
Adelman-McCarthy J. K. et al., 2006, ApJS, 162, 38
Alexander D. R., Ferguson J. W., 1994, ApJ, 437, 879
Alves-Brito A. et al., 2006, A&A, 460, 269
Annibali F., Bressan A., Rampazzo R., Zeilinger W. W., Danese L., 2007, A&A, 463, 455
Balogh M. L., Morris S. L., Yee H. K. C., Carlberg R. G., Ellingson E., 1999, ApJ, 527, 54
Barbuy B., 1994, ApJ, 430, 218
Barbuy B., Perrin M.-N., Katz D., Coelho P., Cayrel R., Spite M., Van't Veer-Menneret C., 2003, A&A, 404, 661
Barklem P. S., Stempels H. C., Allende Prieto C., Kochukhov O. P., Piskunov N., O'Mara B. J., 2002, A&A, 385, 951
Bell R. A., Paltoglou G., Tripicco M. J., 1994, MNRAS, 268, 771
Bensby T., Feltzing S., Lundström I., Ilyin I., 2005, A&A, 433, 185
Bernkopf J., 1998, A&A, 332, 127
Borges A. C., Idiart T. P., de Freitas Pacheco J. A., Thevenin F., 1995, AJ, 110, 2408
Bressan A., Fagotto F., Bertelli G., Chiosi C., 1993, A&AS, 100, 647
Brodie J. P., Hanes D. A., 1986, ApJ, 300, 258
Brott I., Hauschildt P. H., 2005, in Turon C., O'Flaherty K. S., Perryman M. A. C., eds, ESA SP-576: The Three-Dimensional Universe with *Gaia*: A PHOENIX Model Atmosphere Grid for *Gaia*. p. 565
Bruzual A. G., 1983, ApJ, 273, 105
Bruzual G., Charlot S., 2003, MNRAS, 344, 1000 (BC03)
Burstein D., Faber S. M., Gaskell C. M., Krumm N., 1984, ApJ, 287, 586
Canuto V. M., Mazzitelli I., 1992, ApJ, 389, 724
Cassisi S., Salaris M., Castelli F., Pietrinferni A., 2004, ApJ, 616, 498
Castelli F., Kurucz R. L., 2003, in Piskunov N., Weiss W. W., Gray D. F., eds, IAU Symp. 210, Modelling of Stellar Atmospheres: New Grids of ATLAS9 Model Atmospheres. Astron. Soc. Pac., San Francisco, p. A20 (ATLAS9)
Castelli F., Kurucz R. L., 2004, A&A, 419, 725
Caughlan G. R., Fowler W. A., 1988, At. Data Nucl. Data Tables, 40, 283
Caughlan G. R., Fowler W. A., Harris H. J., Zimmerman B. A., 1985, At. Data Nucl. Data Tables, 32, 197
Cayrel R., Faurobert-Scholl M., Feautrier N., Spielfieldel A., Thevenin F., 1996, A&A, 312, 549
Cayrel R. et al., 2004, A&A, 416, 1117
Cenarro A. J., Gorgas J., Cardiel N., Vazdekis A., Peletier R. F., 2002, MNRAS, 329, 863
Cenarro A. J. et al., 2007, MNRAS, 374, 664
Chabrier G., 2003, PASP, 115, 763
Charbonnel C., 1994, A&A, 282, 811
Cid Fernandes R., Mateus A., Sodré L., Stasińska G., Gomes J. M., 2005, MNRAS, 358, 363
Coelho P., Barbuy B., Melendez J., Schiavon R., Castilho B., 2005, A&A, 443, 735 (C05)
Colless M. et al. 2001, MNRAS, 328, 1039
Delgado R. M. G., Cerviño M., Martins L. P., Leitherer C., Hauschildt P. H., 2005, MNRAS, 357, 945
Diaz A. I., Terlevich E., Terlevich R., 1989, MNRAS, 239, 325
Ferguson J. W., Alexander D. R., Allard F., Barman T., Bodnarik J. G., Hauschildt P. H., Heffner-Wong A., Tamanai A., 2005, ApJ, 623, 585
Fuhrmann K., Axer M., Gehren T., 1993, A&A, 271, 451
Gallazzi A., Charlot S., Brinchmann J., White S. D. M., Tremonti C. A., 2005, MNRAS, 362, 41
Girardi L., Bressan A., Bertelli G., Chiosi C., 2000, A&AS, 141, 371
Girardi L., Bertelli G., Bressan A., Chiosi C., Groenewegen M. A. T., Marigo P., Salasnich B., Weiss A., 2002, A&A, 391, 195
González J. J., 1993, PhD thesis, Univ. California
Grevesse N., Sauval A. J., 1998, Space Sci. Rev., 85, 161
Groenewegen M. A. T., 2006, A&A, 448, 181
Gustafsson B., Edvardsson B., Eriksson K., Jørgensen U. G., Mizuno-Wiedner M., Plez B., 2003, in Piskunov N., Weiss W. W., Gray D. F., eds, IAU Symp. 210, Modelling of Stellar Atmospheres. Astron. Soc. Pac., San Francisco, p. A4
Haft M., Raffelt G., Weiss A., 1994, ApJ, 425, 222
Hinkle K., Wallace L., Valenti J., Harmer D., 2000, in Hinkle K., Wallace L., Valenti J., Harmer D., eds, Visible and Near Infrared Atlas of the Arcturus

Spectrum 3727–9300 Å. Astron. Soc. Pac., San Francisco, ISBN: 1-58381-037-4

Houdashelt M. L., Trager S. C., Worthey G., Bell R. A., 2002, BAAS, 34, 1118

Iben I. J., 1967, ARA&A, 5, 571

Iglesias C. A., Rogers F. J., 1996, ApJ, 464, 943

Itoh N., Hayashi H., Nishikawa A., Kohyama Y., 1996, Astrophys. J. Suppl. Ser., 102, 411

Jorgensen U. G., Carlsson M., Johnson H. R., 1992, A&A, 254, 258

Kelson D. D., Illingworth G. D., Franx M., van Dokkum P. G., 2006, ApJ, 653, 159

Korn A. J., Maraston C., Thomas D., 2005, A&A, 438, 685

Kurucz R. L., 1992, Rev. Mex. Astron. Astrofis., 23, 45

Kurucz R. L., 2006, in Stee P., ed., EAS Publications Series Including all the Lines. EDP Sciences, Les Ulis, p. 129

Kurucz R. L., Furenlid I., Brault J., Testerman L., 1984, Solar Flux Atlas from 296 to 1300 nm. National Solar Observatory Atlas, Sunspot. National Solar Observatory, New Mexico

Le Borgne J.-F. et al., 2003, A&A, 402, 433

Le Borgne D., Rocca-Volmerange B., Prugniel P., Lançon A., Fioc M., Soubiran C., 2004, A&A, 425, 881

Lecureur A., Hill V., Zoccali M., Barbuy B., Gomez A., Minniti D., Ortolani S., Renzini A., 2007, A&A, 465, 799

Lee H.-c., Worthey G., 2005, ApJS, 160, 176

Lejeune T., Cuisinier F., Buser R., 1997, A&AS, 125, 229

Lejeune T., Cuisinier F., Buser R., 1998, A&AS, 130, 65

Malagnini M. L., Franchini M., Morossi C., di Marcantonio P., 2005, in Turon C., O'Flaherty K. S., Perryman M. A. C., eds, The Three-Dimensional Universe with Gaia. ESA, Noordwijk, p. 595

Marigo P., Girardi L., 2007, A&A, 469, 239

Martins L. P., Coelho P., 2007, MNRAS, in press

Martins L. P., Delgado R. M. G., Leitherer C., Cerviño M., Hauschildt P., 2005, MNRAS, 358, 49

Mathis H., Charlot S., Brinchmann J., 2006, MNRAS, 365, 385

Mendes de Oliveira C., Coelho P., González J. J., Barbuy B., 2005, AJ, 130, 55

Munari U., Sordo R., Castelli F., Zwitter T., 2005, A&A, 442, 1127

Panter B., Heavens A. F., Jimenez R., 2003, MNRAS, 343, 1145

Pietrinferni A., Cassisi S., Salaris M., Castelli F., 2006, ApJ, 642, 797

Piovan L., Tantalo R., Chiosi C., 2003, A&A, 408, 559

Plez B., 1992, A&AS, 94, 527

Prochaska L. C., Rose J. A., Schiavon R. P., 2005, AJ, 130, 2666

Proctor R. N., Sansom A. E., 2002, MNRAS, 333, 517

Proctor R. N., Forbes D. A., Beasley M. A., 2004, MNRAS, 355, 1327

Reddy B. E., Tomkin J., Lambert D. L., Allende Prieto C., 2003, MNRAS, 340, 304

Rogers F. J., Swenson F. J., Iglesias C. A., 1996, ApJ, 456, 902

Rose J. A., 1985, AJ, 90, 1927

Salaris M., Weiss A., 1998, A&A, 335, 943

Salasnich B., Girardi L., Weiss A., Chiosi C., 2000, A&A, 361, 1023

Salpeter E. E., 1955, ApJ, 121, 161

Sánchez-Blázquez P. et al., 2006, MNRAS, 371, 703

Schiavon R., 2007, ApJS, 171, 146

Smith R. J., Hudson M. J., Lucey J. R., Nelan J. E., Wegner G. A., 2006, MNRAS, 369, 1419

Tantalo R., Chiosi C., 2004, MNRAS, 353, 917

Thomas D., Maraston C., Bender R., 2003a, MNRAS, 343, 279

Thomas D., Maraston C., Bender R., 2003b, MNRAS, 339, 897

Thomas D., Maraston C., Korn A., 2004, MNRAS, 351, L19

Trager S. C., Worthey G., Faber S. M., Burstein D., Gonzalez J. J., 1998, ApJS, 116, 1

Trager S. C., Faber S. M., Worthey G., González J. J., 2000, AJ, 119, 1645

Tripicco M. J., Bell R. A., 1995, AJ, 110, 3035

Valdes F., Gupta R., Rose J., Singh H., Bell D., 2004, ApJS, 152, 251

VandenBerg D. A., Swenson F. J., Rogers F. J., Iglesias C. A., Alexander D. R., 2000, ApJ, 532, 430

van't Veer-Menneret C., Megessier C., 1996, A&A, 309, 879

Vazdekis A., 1999, ApJ, 513, 224

Vazdekis A., Cenarro A. J., Gorgas J., Cardiel N., Peletier R. F., 2003, MNRAS, 340, 1317

Weiss A., Schlattl H., 2000, A&AS, 144, 487

Weiss A., Peletier R. F., Matteucci F., 1995, A&A, 296, 73

Weiss A., Salaris M., Ferguson J. W., Alexander D. R., 2007, in Vazdekis A., Peletier R. F., eds, IAU Symp. 241, Stellar Populations as Building Blocks of Galaxies: α-Element Enhanced Opacity Tables and Low-mass Metal-rich Stellar Models. Cambridge Univ. Press, Cambridge

Westera P., Lejeune T., Buser R., Cuisinier F., Bruzual G., 2002, A&A, 381, 524

Worthey G., 1998, PASP, 110, 888

Worthey G., Ottaviani D. L., 1997, ApJS, 111, 377

Worthey G., Faber S. M., Gonzalez J. J., 1992, ApJ, 398, 69

Worthey G., Faber S. M., Gonzalez J. J., Burstein D., 1994, ApJS, 94, 687

Zhang F., Li L., Han Z., 2005, MNRAS, 364, 503

Zoccali M. et al., 2004, A&A, 423, 507

SUPPLEMENTARY MATERIAL

The following supplementary material is available for this article.

Appendix A. Predictions of the effect of an α enhancement on broad-band colours and spectral indices: Tables 1–19.

This material is available as part of the online article from: http://www.blackwell-synergy.com/doi/abs/10.1111/j.1365-2966.2007.12364.x
(This link will take you to the article abstract.)

Please note: Blackwell Publishing are not responsible for the content or functionality of any supplementary materials supplied by the authors. Any queries (other than missing material) should be directed to the corresponding author for the article.

This paper has been typeset from a T$_E$X/L^{A}T$_E$X file prepared by the author.